

Chapter 2

In Situ TEM Method and Materials

In 1959, Nobel laureate Richard Feynman gave a speech entitled “There’s Plenty of Room at the Bottom”. In his speech, he talked about the manipulation and control of materials on a small length scale, such as the fabrication of molecular machines. In 1982, Binnig et al. invented scanning tunneling microscope (STM) [1]. In 1990, Eigler et al. demonstrated the ability of arranging atoms and put 35 Xe atoms on the surface of Ni crystal patterned as “IBM” [2]. However, STM is based on the tunneling current and requires a conductive surface. Binnig et al. invented atomic force microscopy (AFM) [3], which is based on the interacting forces between the scanning probe and sample surface. Recently, the resolution and manipulation precision of AFMs has reached atomic level [4]. What scanning probe microscopy (SPM) has in common is that the observations and manipulations are limited to the surface, lacking insights into the structural mechanisms. In addition, scanning is involved for both imaging and manipulation, which limits the efficiency. As already been introduced in Chap. 1, TEM is a powerful tool for the materials structural characterizations with atomic resolution. In recent years, it is possible to combine SPM with TEM to conduct high-resolution structural characterizations in three dimensions and precise manipulations of nanomaterials simultaneously [5].

In this thesis, in situ TEM-SPM techniques are used for the investigation of CNTs growth mechanism and fabrication of CNTs-based devices. In the following sections, the method will be introduced, including a short introduction of TEM with an emphasis on the interactions between electrons and materials, principles and functions of the TEM-SPM platform, first principles calculations, and design and fabrication of materials for the in situ experiments.

2.1 Interactions Between Electrons and Materials

TEM is a microscopic technique by using an electron beam transmitted through thin samples. According to the Abbe theory, TEM has the potential of extremely high subatomic resolution because of the short wavelength. The signals generated from the interactions between electrons and materials could be collected to get structural

information, such as the morphology, crystalline phase structure, chemical bonding, composition, and so on. Since the invention of TEM by Knoll and Ruska in 1931, great progresses have been made in achieving higher resolution by increasing the accelerating voltage, improving the electromagnetic lens, and adopting the charge-coupled device (CCD) cameras for imaging. In addition, the 4D techniques developed by Zewail et al. enable the extremely fast processes in the range of femto-seconds [6]. In this thesis, the imaging function of TEM is used to record the structural evolutions; electron energy loss spectroscopy (EELS) and energy-dispersive X-ray spectroscopy (EDS) are applied to analyze the composition; and the interaction between electrons and materials are utilized for high precision machining.

2.1.1 Elastic Interactions

The interactions between electrons and materials include elastic and inelastic scattering. For the elastically scattered electrons, only the directions are changed, while for inelastically scattered electrons, both the direction and energy are changed. Elastically scattered electrons are involved in the formation of images, diffraction patterns, while inelastically scattered electrons contribute to the EELS and EDS.

The optical path diagrams for the different modes in TEM could be changed for different purposes. The electron beam emitted by the electron gun is transformed to be parallel by condenser lenses and reaches the surface of the sample. Most of the electrons transmit directly as the direct beam. The elastically scattered electrons form diffraction patterns on the focal plane, and form images on the image plane. By changing the current in the intermediate lens, a diffraction pattern or image is selected for further magnification and projected by the projection lens onto the CCD camera or negative films.

There are three types of imaging mechanisms and corresponding contrasts. The first type is the mass-thickness contrast, which is based on the differences of absorption of electrons in materials. The second type is diffraction contrast, which is based on the differences of diffraction of electron beams from different crystalline structures and different orientations. The third type is phase contrast for HRTEM images, which is based on the interferences of the direct beam and diffracted beams. The atomic structures such as the lattice constants and defects could be directly resolved in the HRTEM images. In this thesis, all the three contrasts are involved. For example, the mass-thickness contrast is used for the observation of morphologies and alignment of the probes. The diffraction contrast is used for the determination of phase structures of the filled metals. And the HRTEM images are used for the observation of atomic processes.

2.1.2 Inelastic Interactions

Besides elastic interactions, the high-energy electron beams also have strong inelastic interactions with the materials, including the secondary electrons, X-rays, and irradiation effects, and so on. The secondary electrons and X-rays are involved in

the following one process. Because of inelastic scattering, part of the energy is transferred to the inner orbital electrons in the materials, resulting in the releasing of secondary electrons. Electrons in the higher energy orbital jump to the lower orbital and emit X-rays in the meantime. The excitation and emission are both related to the featured energy levels of elements and chemical bonding, therefore, the composition of the materials could be obtained by collecting the X-rays or measuring the energy loss of the transmitted electrons.

The above-mentioned elastic and inelastic interactions do not induce structural changes, while electron beam irradiation effects can alter the structure by transferring kinetic energy to the atoms [7–9]. Irradiation effects include four types: The first type is decomposition, which mainly happens in polymers. The long chain structure is destroyed by the ionization effect. The second type is heating effect, because of the interaction of incident electrons and phonons in the materials. The heating effect is strongly associated with the chemical bonding of the samples. For metals with high thermal conductivity, the heating effect is around several kelvins and negligible in normal cases. For ceramics and polymers with poor thermal conductivity, the temperature rise could be as much as 1000 K. In this thesis, because of the good thermal conductance of CNTs and filled metals, the heating effects are negligible. The third irradiation effect is knock-on effect, by which the atoms in the crystal lattices are knocked-off the equilibrium positions. This effect could be described by the following formula, $E_t = [\sqrt{100 + AE_d/5} - 10]/20$, where E_d is the energy of the incident beam, E_t is the transferred energy, and A is a constant associated with the element. For each element, there is threshold energy that the atom could be knocked-off. Generally, lighter elements have lower threshold energy. For example, carbon and iron atoms could be knocked out by an incident beam of 80 kV and 400 kV, respectively. In this thesis, the accelerating voltage is 200 kV or 300 kV, which can destroy the carbon shells and is not high enough to knock off the metal atoms, therefore realizing element-selective etching for the fabrication of CNT-clamped MACs. Also the technique is used for the injection of carbon atoms into the nano furnaces. Another electron irradiation effect is the surface sputtering. Because of the unsaturated chemical bonding on the surface, the threshold energy for displacing atoms is lower than that of bulk. Take Fe as an example, the energy barrier for bulk lattice and surface atoms are 16 eV and 4–8 eV, respectively. The energy transferred to Fe atoms from 200 kV and 300 kV electron beams are 9.4 eV and 15.3 eV, respectively, which is enough to knock off the surface atoms. In this thesis, the surface sputtering effects are involved in the thinning of exposed metal nanowires.

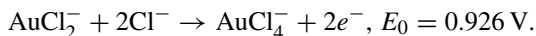
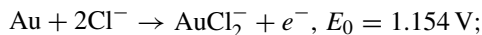
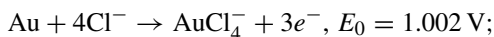
2.2 TEM-SPM In Situ Platform

In this thesis, a commercial TEM-SPM in situ platform from Nanofactory is used, including TEM-STM type for electrical measurements and TEM-AFM type for mechanical measurements. In the following parts, the configuration and functions of the platform will be introduced.

There are four main parts included in the TEM-SPM platform: a sample holder with a 3D piezo-motor, an electrical and mechanical testing system, and the control software. The signals of movements and bias are controlled by the software and sent through the control box and amplifier, and then to the probes inside the TEM. The measured currents and forces signals are collected inside the TEM, amplified and then sent back to the user interface on the computer. In the meantime, structural and compositional information is recorded the same as the normal TEM. Realtime structural evolutions are recorded by a CCD camera.

The difference in holder between this platform and normal TEM is the structure of the head. Instead of a hole for placing thin foils, a piezo tube connected ceramic ball and a hole are placed in the TEM-STM holder for the probe and the samples. For the TEM-AFM holder, a TEM cantilever is placed at the opposite side of the piezo tube. Therefore, by moving the probe against the cantilever, corresponding deflection and forces could be recorded. There is no difference in the overall outer shape and dimensions; therefore, the in situ holders are compatible with normal TEM. And tilting, selected area electron diffraction pattern (SAED), EDS, and EELS could be operated as normal.

A critical part of the TEM-SPM platform is the probe, because the size of the probe determines the length scale of the investigation system, and the contact between the probe and the sample determines contact resistance and reliability. The probes in this thesis are produced using a traditional electrochemical etching method [10]. The optimized parameters are as follows: DC bias 5 V, 1:1 hydrochloric acid (HCl), immersion length in electrolyte: 4 mm, counter electrode: gold wire, and etching time: 5 min. During the etching, the following reactions take place [11]:

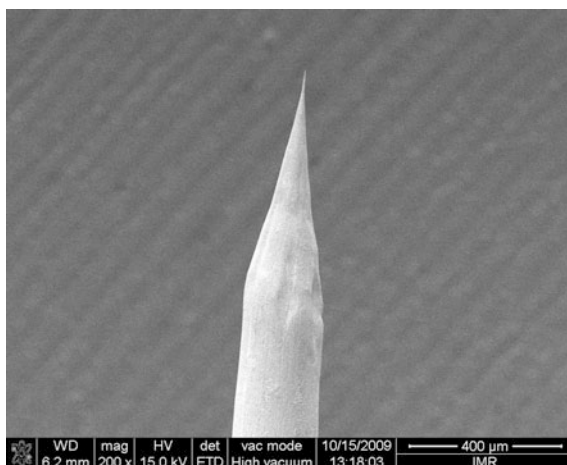


The etching speed at the liquid–air interface is fastest because the immersed part is coated with a viscous layer from the reactions. The wire will be disconnected by the weight of the immersed part when it is etched thin enough. Then the etched tips are cleaned by flushing water to stop further etching. The tips produced under optimized conditions could be as sharp as 50 nm in radius, as demonstrated by the SEM image (Fig. 2.1).

There are two modes for the movement control of the scanning probe. One is the coarse mode driven by vibration and inertial movements, with the movement range as large as 1 mm, so as to align the probe with the sample roughly. The other is the fine mode based on the piezoelectric principle, with very high precision up to 0.2 Å in the up/down and left/right directions and 0.025 Å in the backward/forward direction.

When the probe and sample are aligned precisely, various functions could be realized by applying corresponding stimuli. For example, the basic functions of electrical and mechanical measurements could be carried out by applying bias and moving against the AFM cantilever, respectively. In addition, the combination of Joule heating-induced high temperature, electromigration, electric field, and

Fig. 2.1 SEM image of the tip of a Au probe



electron beam irradiation could realize more complicated functions. In the following parts, some examples will be presented to introduce the main functions of the TEM-SPM platform.

First, it is possible to measure the intrinsic electrical properties of nanostructures and associate them with the HRTEM images. The applied bias range is ± 10 V (± 140 V for field emission option), and the measurement noise is around 1 nA, depending on the circumstances. Jin et al. investigated the field emission of single CNTs by applying a high voltage between the probe and the CNT with a narrow gap [12]. It was found that along with the field emission, structural evolutions took place for the cap of the CNT, which was attributed as the degradation of the emitted currents. By passing a current, high temperature up to 2000 K could be obtained by Joule heating effect, and Huang et al. used this technique to study the deformation of CNTs at high temperature [13]. Superplasticity up to 280 % elongation was observed for SWCNTs.

Another basic function of the TEM-SPM platform is mechanical measurements. The noise of the measured force is at the nanoNewton level. Therefore, the force–displacement relationship of extremely small nanostructures could be tested. Golberg group in NIMS did systematic researches on the mechanical properties of 1D materials. For examples, it was found that under small bending angles, boron nitride (BN) nanotubes could be bent repeatedly and elastically, with the elastic modulus of 0.5–0.6 TPa, while permanent deformation occurred when the bending angle was larger than 115° , following the kink mechanism with buckling between the nanotube walls [14].

Besides the basic functions, various manipulations could be realized by the combination of electron beam irradiation, current, force, and so on. Svensson et al. used single CNTs as nanoscale pipettes to transfer nanoparticles by reversing the current direction and correspondingly the interaction forces [15]. Cumings et al. peeled off the outer layers of a MWCNT with Joule heating-induced high temperature and the inner parts of the CNT could be retracted and inserted like a

nanoscale piston [16]. Sun et al. combined the electron beam irradiation and Joule heating to shrink a nanotube and applied a high pressure on the filled metals to observe the structural evolutions [17].

2.3 First Principles Calculations

The advantages of in situ TEM are the real-time observations of the structural evolutions and correlations with the properties measurements. However, critical questions such as the driving force could not be answered by using in situ TEM alone. In addition, the recorded TEM images are two-dimensional projection of the three-dimensional structure. Therefore, it is difficult to capture the structural evolutions comprehensively. Another shortcoming of in situ TEM is the limited temporal resolution. To acquire a TEM image, it takes at least 0.05 s, which is not short enough to record the fast processes. Therefore, in this thesis, theoretical calculations are used to complement the in situ TEM study. Proper structural models are built according to the TEM observations. And by comparing the total energy, stability of possible structures and evolution paths, the possible structural mechanisms could be revealed. In addition, the electric properties could be predicted and compared with the experimental results.

In this thesis, first principles calculations based on density functional theory (DFT) are used, and generalized gradient approximation (GGA) is adopted to describe the electronic exchange–correlation interactions [18]. All the calculations are conducted with the full-potential projector augmented-wave (PAW) method [19] in Vienna ab initio simulation package (VASP) [20]. Take the formation process of metal atomic chains as an example (110) (111) and (001) oriented nanowires were constructed for BCC structured Fe, FCC structured Pt and HCP structured Co, respectively. Tensile elongation with a step of 0.4 Å was applied on the atoms at the end surfaces. After each step, full structural relaxation was carried out. The total energy was calculated after the formation of single atomic chains. After that the charge density distributions were calculated to predict the nature of the chemical bonding and spin-resolved density states were computed to predict the electronic properties.

2.4 Design and Fabrication of Samples for In Situ TEM

The samples for in situ TEM are not only the objects of investigations but also important functional components. There are certain restrictions on samples in TEM, such as thickness and stability under high vacuum. Therefore, it is necessary to design both the structure and fabrication methods. In this thesis, most of the experiments are based on filled CNTs as summarized in Table 2.1, which were produced by CVD or AAO template methods.

Table 2.1 Summary of the samples in this work

Sample	Fabrication method	Structural features	Functions	Subject
Fe ₂ O ₃ -filled CNT	AAO template	Metal catalyst filled in CNT	Growth furnace, metallic catalyst	CNTs growth mechanism
SiO _x -filled CNT	AAO template	Metal free catalyst in CNT	Growth furnace, non-metallic catalyst	
Fe-filled CNT	FCCVD	Fe-filled CNT	CNT sheath during fabrication;	CNT-clamped MAC
Fe–Ni-filled CNT	FCCVD	Fe alloy-filled CNT	Mechanical clamp during tension;	
Pt-filled CNT	AAO template	Non-traditional metal for CNT growth	Electrical leads during IV test	

2.4.1 CVD Method

Fe-filled CNTs were produced by using acetylene (C₂H₂) as the carbon source, ferrocene (Fe(C₅H₅)₂) as the catalyst precursor at 860 °C. The CNTs are highly aligned with high purity, as revealed by the SEM image (Fig. 2.2a). TEM image (Fig. 2.2b) demonstrates that the CNTs are uniform in diameter and with high percentage of Fe filling. The filled Fe nanowires are about 200–300 nm in length. HRTEM image (Fig. 2.2c) shows the high crystallinity with clear lattices corresponding to body-cubic centered (BCC) structured Fe.

Chlorine was found to be able to etch carbon during the growth of CNTs by Lv et al. [21], and therefore high percentage metal-filled CNTs could be obtained. With this technique, Fe alloys-filled CNTs were grown by using a mixture of ferrocene, nickelocene, and cobaltocene as the catalyst precursor. The optimized growth conditions are: the solution of the precursors in trichlorotoluene with the concentration of 10 % is injected into the growth furnace with a speed of 0.15 μl/min. The growth temperature is 860 °C. The flow rates for Ar and H₂ are 1500 and 300 ml/min, respectively.

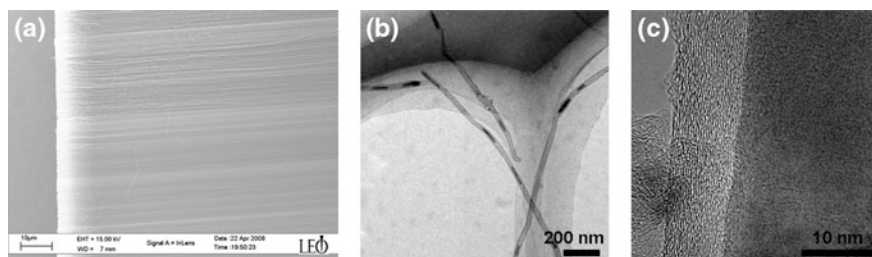


Fig. 2.2 Structure of the Fe-filled CNTs by FCCVD method using acetylene as carbon source. **a** SEM image. **b–c** Low-magnification and high-resolution TEM images

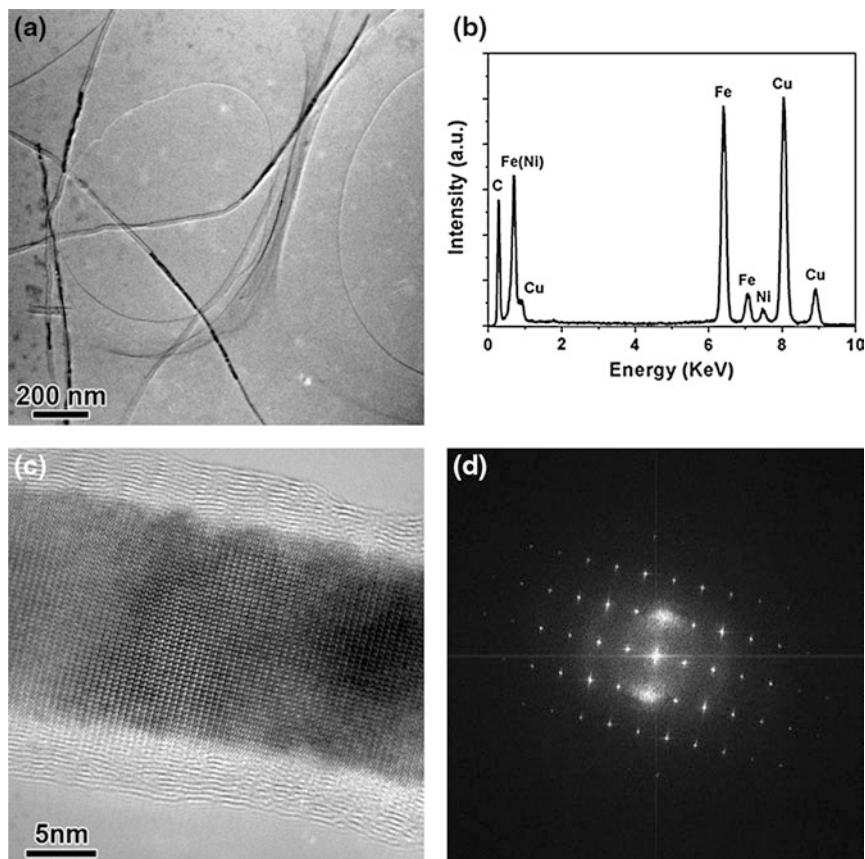


Fig. 2.3 Structure of the Fe–Ni alloy-filled CNTs by FCCVD method using chloride-included carbon source: **a** TEM image, **b** EDS spectrum, **c** High resolution TEM image, **d** FFT pattern of (c) [22]

Figure 2.3 shows the characterization results of the Fe–Ni alloy-filled CNTs. Compared with previous results of Fe-filled CNTs, the filling ratio and length are both increased. Fe, Ni, C, and Cu signals are detected by EDS, where Cu comes from the TEM grid. Because of the etching of chlorine, the walls of the CNTs are much thinner (Fig. 2.3c). Both the HRTEM image and FFT pattern (Fig. 2.3d) confirm the single crystalline nature of the filled alloy.

2.4.2 AAO Template Method

By using CVD method in the previous section, the filling of CNTs is limited to the catalyst metals, typically Fe-group metals and alloys. While various metals could be filled into CNTs by using the AAO template method, which will be

Table 2.2 Experimental parameters of SiO_x , Fe_2O_3 , and Pt-filled CNTs by using AAO template method

Material	Catalog	Step one	Step two	Step three
SiO_x	Non-metal oxide	Production of AAO template	CNTs deposition	SiO_x deposition
Fe_2O_3	Metal oxide		CNTs deposition	$\text{Fe}(\text{NO}_3)_3$ decomposition
Pt	Noble metal		Pt nanowire deposition	CNT deposition

introduced in this section [23]. Pt, Fe_2O_3 , and SiO_x -filled CNTs were produced by the method, as summarized in Table 2.2.

The first step was the fabrication of AAO template, with the following procedure:

1. Initial electrochemical oxidation of Al foils (99.99 %) at 20 V DC in 10 %wt H_2SO_4 , at 10 °C for 2 h.
2. Remove the initial oxidation layer in H_3PO_4 at 60 °C to get an ordered pattern.
3. Secondary electrochemical oxidation with the same parameters for 4 h to get AAO template with one end open.
4. Open the other end by further anodic oxidation in a mixed electrolyte of HClO_4 and acetone (2:1) at 25 V for 1–3 min.

The second step for the preparation of filled CNTs by using AAO template method was the deposition of CNTs in the pores of the templates, with the following procedure:

1. Put the AAO template in the middle of a vertical CVD furnace; increase the temperature to 650 °C with a speed of 10 °C/min under N_2 flow (100 sccm).
2. Deposition of carbon at 650 °C by using C_2H_2 as the carbon source (10 sccm) and Ar as the carrier gas (100 sccm).
3. Annealing at 750 °C in N_2 for 3 h to enhance the crystalline order of the deposited carbon layers.
4. Remove the AAO template in NaOH solution (5 M) to get free standing CNTs.

The third step was to use a CVD method for the filling of SiO_x in CNTs with the following procedure:

1. Put the AAO template in the middle of a vertical CVD furnace; increase the temperature to 500 °C with a speed of 10 °C/min under N_2 flow (100 sccm).
2. Deposition of SiO_x at 500 °C, by using SiH_4 as the silicon source (10 sccm) and Ar as the carrier gas (40 sccm). During the deposition, trace amount of O_2 is introduced into the furnace to get SiO_x .

Figure 2.4 shows the TEM image of the SiO_x -filled CNTs. The CNTs fabricated from AAO templates are highly uniform in diameter and are filled with SiO_x particles. The CNTs are poor crystalline as revealed by the curved and non-continuous lattices. The SiO_x particles are 5–10 nm in diameter. HRTEM image reveals that the particles are amorphous and free of carbon coating.

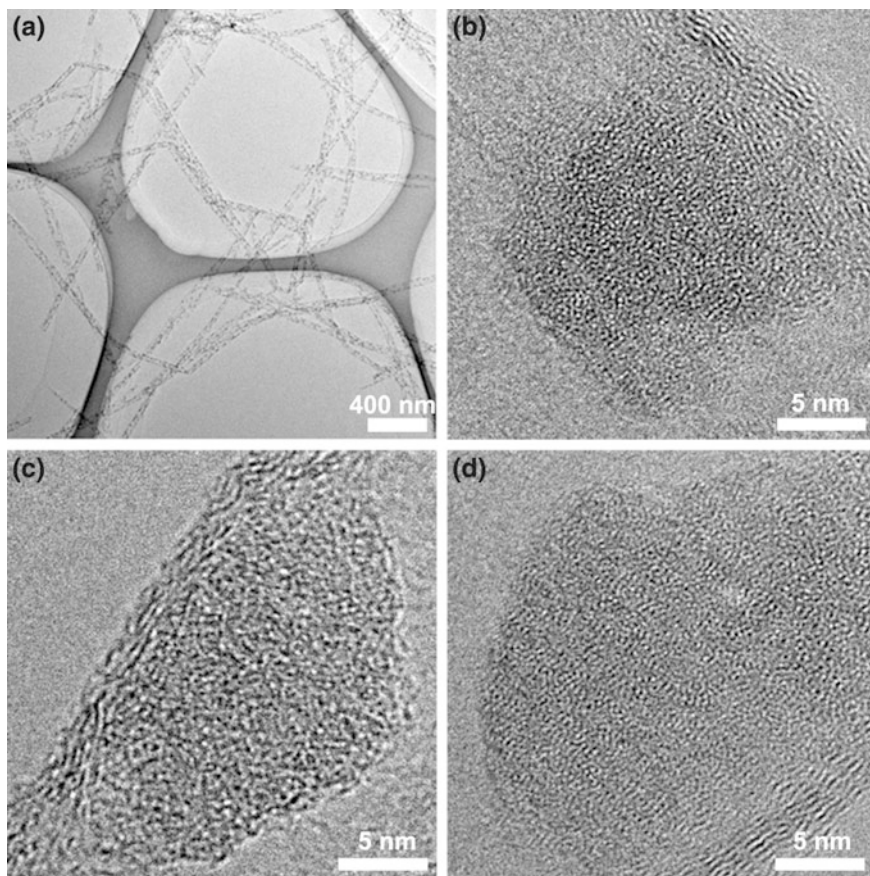


Fig. 2.4 Structural characterizations of the SiO_x-filled CNTs by using AAO template method: **a** TEM image, **b–d** High-resolution TEM images. Reprinted with the permission from Ref. [24]. Copyright 2011, American Chemical Society

The filling of Fe₂O₃ into CNTs was realized by a decomposition method, with the following procedure:

1. Immerse AAO template in the ethanol solution of Fe(NO₃)₃ at 80 °C for 30 min to get the precursor of Fe₂O₃ and then washed by deionized water.
2. Decomposition of the Fe(NO₃)₃ in AAO template at 350 °C in N₂ for 6 h.

Similar to the SiO_x-filled CNTs, the CNTs are uniform in diameter and the filling rate is very high. But the filled Fe₂O₃ nanoparticles are single crystalline, which is different from SiO_x. The diameters of the CNT and Fe₂O₃ particles are 50–60 nm and 5–10 nm, respectively.

Pt was filled into CNTs following another route by electrochemical deposition, with the following procedure:

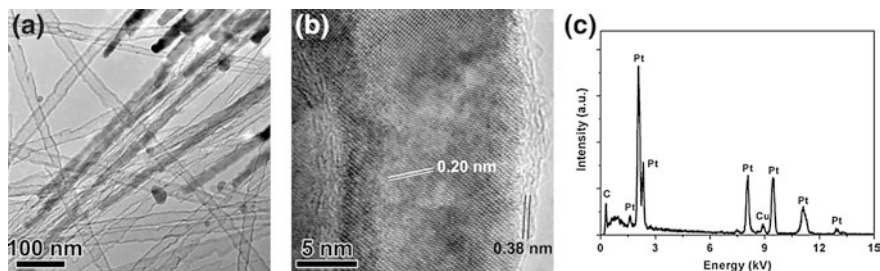


Fig. 2.5 Structure of the Pt-filled CNTs by AAO template method: **a** TEM image, **b** High-resolution TEM image, **c** EDS spectrum [22]

1. A layer of silver is deposited on one side of the AAO template as the electrode for further electrochemical deposition.
2. Electrochemical deposition of Pt using a three electrode system at -0.5 V for 1 h in the electrolyte of a mixture of H_2PtCl_6 (1.0 g/L) and H_3BO_3 (25 g/L).

Figure 2.5 shows the structure of Pt-filled CNTs. The CNTs are uniform in diameter and length. About 40 % of the CNTs are filled continuously. HRTEM image shows that the CNTs have very thin walls with only 3–5 layers. The filled Pt nanoparticles are single crystalline with lattices corresponding to Pt (111) as clearly identified. The composition was checked by EDS, and strong signals from Pt, C from Pt-filled CNTs, and Cu from TEM grids were detected.

2.5 Summary

Nano-lab inside TEM is an important research topic at the frontiers of nanoscience and nanotechnology, because of its atomic resolution, rich functions for measurement, and manipulations. In this chapter, the principle and method of in situ TEM-SPM technique is introduced, including the interactions between electrons and materials, functions of TEM-SPM in situ holders, first principles calculations, and fabrication of designated samples. The in situ platform combines the normal structural characterizations of TEM, materials processing functions by electron irradiation, various stimuli by the in situ holders, and theoretical calculations to provide in-depth understanding of the structural mechanism. The design and fabrication of suitable samples with specified structures and functions is the basis of realizing the functions. It is important to choose the right route for preparing samples according to the purpose of research, and then to select the right tools including experimental and also theoretical models to get a comprehensive understanding.

In Chap. 3, catalysts-filled CNTs are designed for the investigation of the CNTs growth mechanism. AAO template and CVD method are chosen for the filling of different kinds of catalyst. With Joule heating-induced high temperature and electron beam irradiation-induced carbon atoms injection, the growth of CNTs could

be observed in situ. To realize the in situ investigations of the all-carbon growth of CNTs, carbon micro coils are designed, and high current-induced electromigration and Joule heating-induced high temperature are used to provide driving force.

In Chap. 4, metal-filled CNTs are designed for the fabrication of CNT-clamped MACs, and produced by using floating CVD and AAO template methods, depending on the chemical properties of the metals. Then element-selective electron beam irradiation is used for the peeling off of the carbon shells and surface sputtering is used to etch the metal nanowires. After that, tension is applied to elongate the nanowire and produce MACs. HRTEM and first principles calculations are conducted to study the formation process and the electrical properties of the fabricated CNT-clamped MACs are tested by using the TEM-STM in situ holder.

References

1. Binnig G, Rohrer H, Gerber C, Weibel E (1982) Tunneling through a controllable vacuum gap. *Appl Phys Lett* 40:178–180
2. Eigler DM, Schweizer EK (1990) Positioning single atoms with a scanning tunnelling microscope. *Nature* 344:524–526
3. Binnig G, Quate CF, Gerber C (1986) Atomic force microscope. *Phys Rev Lett* 56:930
4. Custance O, Perez R, Morita S (2009) Atomic force microscopy as a tool for atom manipulation. *Nat Nano* 4:803–810
5. Banhart F (2008) *In-situ electron microscopy at high resolution*. World Scientific, Singapore
6. Zewail AH (2010) Four-dimensional electron microscopy. *Science* 328:187–193
7. Egerton RF, Li P, Malac M (2004) Radiation damage in the TEM and SEM. *Micron* 35:399–409
8. Egerton RF, Wang F, Crozier PA (2006) Beam-induced damage to thin specimens in an intense electron probe. *Microsc Microanal* 12:65–71
9. Williams DB, Carter CB (2009) *Transmission electron microscopy: a textbook for materials science*. Springer, New York
10. Eligal L, Culfaz F, McCaughan V, Cade NI, Richards D (2009) Etching gold tips suitable for tip-enhanced near-field optical microscopy. *Rev Sci Instrum* 80:033701
11. Williams C, Roy D (2008) Fabrication of gold tips suitable for tip-enhanced Raman spectroscopy. *J Vac Sci Technol, B* 26:1761–1764
12. Jin CH, Wang JY, Wang MS, Su J, Peng LM (2005) In-situ studies of electron field emission of single carbon nanotubes inside the TEM. *Carbon* 43:1026–1031
13. Huang JY, Chen S, Wang ZQ, Kempa K, Wang YM, Jo SH, Chen G, Dresselhaus MS, Ren ZF (2006) Superplastic carbon nanotubes—Conditions have been discovered that allow extensive deformation of rigid single-walled nanotubes. *Nature* 439:281
14. Golberg D, Costa PMFJ, Lourie O, Mitome M, Bai X, Kurashima K, Zhi C, Tang C, Bando Y (2007) Direct force measurements and kinking under elastic deformation of individual multiwalled boron nitride nanotubes. *Nano Lett* 7:2146–2151
15. Svensson K, Olin H, Olsson E (2004) Nanopipettes for metal transport. *Phys Rev Lett* 93:145901
16. Cumings J, Zettl A (2000) Low-friction nanoscale linear bearing realized from multiwall carbon nanotubes. *Science* 289:602–604
17. Sun L, Banhart F, Krashenninnikov AV, Rodríguez-Manzo JA, Terrones M, Ajayan PM (2006) Carbon nanotubes as high-pressure cylinders and nanoextruders. *Science* 312:1199–1202
18. Wang Y, Perdew JP (1991) Correlation hole of the spin-polarized electron gas, with exact small-wave-vector and high-density scaling. *Phys Rev B* 44:13298

19. Blöchl PE (1994) Projector augmented-wave method. *Phys Rev B* 50:17953
20. Kresse G, Furthmüller J (1996) Efficient iterative schemes for ab initio total-energy calculations using a plane-wave basis set. *Phys Rev B* 54:11169
21. Lv RT, Kang FY, Wang WX, Wei JQ, Gu JL, Wang KL, Wu DH (2007) Effect of using chlorine-containing precursors in the synthesis of FeNi-filled carbon nanotubes. *Carbon* 45:1433–1438
22. Tang D-M, Yin L-C, Li F, Liu C, Yu W-J, Hou P-X, Wu B, Lee Y-H, Ma X-L, Cheng H-M (2010) Carbon nanotube-clamped metal atomic chain. *Proc Natl Acad Sci USA* 107:9055–9059
23. Kyotani T, Pradhan BK, Tomita A (1999) Synthesis of carbon nanotube composites in nano-channels of an anodic aluminum oxide film. *Bull Chem Soc Jpn* 72:1957–1970
24. Liu B, Tang D-M, Sun C, Liu C, Ren W, Li F, Yu W-J, Yin L-C, Zhang L, Jiang C, Cheng H-M (2011) Importance of oxygen in the metal-free catalytic growth of single-walled carbon nanotubes from SiO_x by a vapor–solid–solid mechanism. *J Am Chem Soc* 133:197–199

In Situ Transmission Electron Microscopy Studies of
Carbon Nanotube Nucleation Mechanism and Carbon
Nanotube-Clamped Metal Atomic Chains

Tang, D.-M.

2013, XV, 74 p. 44 illus., 17 illus. in color., Hardcover

ISBN: 978-3-642-37258-2